PHYSICAL REVIEW D **88,** 052004 (2013)

First results on low-mass WIMPs from the CDEX-1 experiment at the China Jinping underground laboratory

W. Zhao,[1] Q. Yue,[1,*] K. J. Kang,[1] J. P. Cheng,[1] Y. J. Li,[1] S. T. Lin,[7,†] Y. Bai,[3] Y. Bi,[5] J. P. Chang,[4] N. Chen,[1] N. Chen,[1] Q. H. Chen,[1] Y. H. Chen,[6] Y. C. Chuang,[7,†] Z. Deng,[1] C. Du,[1] Q. Du,[1] H. Gong,[1] X. Q. Hao,[1] H. J. He,[1] Q. J. He,[1] X. H. Hu,[3] H. X. Huang,[2] T. R. Huang,[7,†] H. Jiang,[1] H. B. Li,[7,†] J. M. Li,[1] J. Li,[1] J. Li,[4] X. Li,[2] X. Y. Li,[3] Y. L. Li,[1] H. Y. Liao,[7,†] F. K. Lin,[7,†] S. K. Liu,[5] L. C. Lü,[1] H. Ma,[1] S. J. Mao,[4] J. Q. Qin,[1] J. Ren,[2] J. Ren,[1] X. C. Ruan,[2] M. B. Shen,[6] L. Singh,[7,8,†] M. K. Singh,[7,8,†] A. K. Soma,[7,8,†] J. Su,[1] C. J. Tang,[5] C. H. Tseng,[7,†] J. M. Wang,[6] L. Wang,[5] Q. Wang,[1] H. T. Wong,[7,†] S. Y. Wu,[6] W. Wu,[3] Y. C. Wu,[1] Y. C. Wu,[4] Z. Z. Xianyu,[1] H. Y. Xing,[5] Y. Xu,[3] X. J. Xu,[1] T. Xue,[1] L. T. Yang,[1] S. W. Yang,[7,†] N. Yi,[1] C. X. Yu,[3] H. Yu,[1] X. Z. Yu,[5] X. H. Zeng,[6] Z. Zeng,[1] L. Zhang,[4] Y. H. Zhang,[6] M. G. Zhao,[3] S. N. Zhong,[3] Z. Y. Zhou,[2] J. J. Zhu,[5] W. B. Zhu,[4] X. Z. Zhu,[1] and Z. H. Zhu[6]

(CDEX Collaboration)

[1]*Key Laboratory of Particle and Radiation Imaging (Ministry of Education) and Department of Engineering Physics, Tsinghua University, Beijing 100084*
[2]*Department of Nuclear Physics, China Institute of Atomic Energy, Beijing 102413*
[3]*School of Physics, Nankai University, Tianjin 300071*
[4]*NUCTECH Company, Beijing 10084*
[5]*School of Physical Science and Technology, Sichuan University, Chengdu 610065*
[6]*YaLong River Hydropower Development Company, Chengdu 610051*
[7]*Institute of Physics, Academia Sinica, Taipei 11529*
[8]*Department of Physics, Banaras Hindu University, Varanasi 221005*
(Received 18 June 2013; published 9 September 2013)

The China Dark Matter Experiment Collaboration reports the first experimental limit on weakly interacting massive particles (WIMPs) dark matter from 14.6 kg-days of data taken with a 994 g p-type point-contact germanium detector at the China Jinping underground laboratory where the rock overburden is more than 2400 m. The energy threshold achieved was 400 eVee. According to the 14.6 kg-day live data, we placed the limit of $\sigma_{\chi N} = 1.75 \times 10^{-40}$ cm^2 at a 90% confidence level on the spin-independent cross section at a WIMP mass of 7 GeV before differentiating bulk signals from the surface backgrounds.

DOI: 10.1103/PhysRevD.88.052004 PACS numbers: 95.35.+d, 29.40.Wk

There are many pieces of evidence from astroparticle physics and cosmology which indicate that about one quarter of the mass of our Universe is composed of dark matter [1]. The nature of dark matter is unknown, except that it is coupled with matter via gravity. One of the possible candidates for dark matter is weakly interacting massive particles (WIMPs, denoted by χ), as motivated by many new theories beyond the standard model [2]. Direct detection of WIMP dark matter has been attempted with different detector technologies in the particle physics domain [3].

In recent years, several experiments have expanded their coverage down to low-mass WIMPs with $m_\chi < 10$ GeV [4–9]. A point-contact germanium detector can reach an energy threshold of hundreds of eV while keeping almost the same energy resolution as the traditional coaxial germanium detector [10]. Thus, it can be a good choice for a low-mass dark matter search. Based on our previous work [11], the China Dark Matter Experiment (CDEX) Collaboration has formally started a program aimed at the direct detection of low-mass WIMPs using a ton-scale germanium array detector system [12]. As the first step, in 2011 the CDEX phase I experiment (CDEX-1) started to test and run its first prototype p-type point-contact germanium (PPCGe) detector with a crystal mass of 994 g. The experiment took place at the China Jinping underground laboratory (CJPL), which was established at the end of 2010. With 2400 m of rock overburden, CJPL is the deepest operational underground laboratory for particle physics in the world. The cosmic ray flux in CJPL is down to 61.7 y^{-1} m^{-2} [13], and this makes it a very good site for ultra-low-background experiments such as dark matter search, double beta decay, and so on.

The point-contact germanium detectors have also been used by several experiments [4,9] to directly search for low-mass WIMPs. Due to the relative shallow cosmic ray shielding, CoGeNT and TEXONO used muon veto detectors to decrease the direct and indirect background contributions from cosmic ray muons. The muon veto method can decrease the background contribution of the

*Corresponding author.
yueq@mail.tsinghua.edu.cn
†Participating as a member of the TEXONO Collaboration.

cosmic rays, but it is less efficient to pick out the background from secondary prompt and delayed cosmogenic radiation. The superior rock shielding of CJPL can minimize the cosmogenic influence. However, it is still important to study the background of a prototype germanium detector to get more knowledge and experience for evaluating and developing a ton-scale experiment with a germanium detector.

In this article, we report the first results from the CDEX-1 experiment. The detailed information about the shielding system was described in Ref. [14]. This phase I experiment did not install any active shielding system such as an anti-Compton detector in order to understand and estimate the background level of the PPCGe detector itself in CJPL, and it will be helpful to compare and learn the background contribution of the anti-Compton detector and its veto efficiency installed in the next experiment phase. The passive shielding system was installed, from outside to inside, as 1 m of polyethylene, 20 cm of lead, 20 cm of borated polyethylene and 20 cm of oxygen-free high-conductivity copper.

Inside the cryostat of the PPCGe detector, the cylindrical germanium crystal has an n^+–type contact on the outer surface and a tiny p^+–type contact as the central electrode. A detailed illustration of the detector, electronics, and data acquisition (DAQ) system as well as its basic performances was also given in Ref. [14]. Signals from the p^+ electrode of the PPCGe were imported into a pulsed reset preamplifier which has three identical energy-related outputs. Two of them were loaded to shaping amplifiers at 6 μs (S_{p6}) and 12 μs (S_{p12}) shaping time, respectively. The discriminator output of S_{p12} supplied the trigger for the DAQ. Another output was distributed to a timing amplifier (T_p) to just amplify the pulse height of the raw traces with a few nanoseconds of shaping time. The pulsed reset preamplifier worked in pulsed mode, so it was reset to its initial condition by discharging the FET quickly marked by one reset inhibit signal. The charge and discharge procedure of the preamplifier are shown in Fig. 1(a), and the reset inhibit signals in Fig. 1(b). The reset inhibit signal was rectangular and quasiperiodic, and the period was typically around 0.7 seconds, which was related to the leakage current of the PPCGe detector. Fig. 1(c) shows the output waveforms from the main amplifier with 12 μs shaping time. The discrimination output of the reset inhibit signal also served as a trigger to record the timing information of the discharging. Signals from the n^+ electrode of the PPCGe were read out by a resistive feedback preamplifier, and then were divided into three identical outputs followed by shaping amplifiers at 2 μs shaping time but different gains. The $S_{p6,12}$, T_p and n^+ electrode outputs were sampled and recorded by a 100 MHz flash analog-to-digital convertor (FADC). The discriminator outputs of the random trigger events (0.05 Hz) from a pulse generator served as a trigger and were digitized as well.

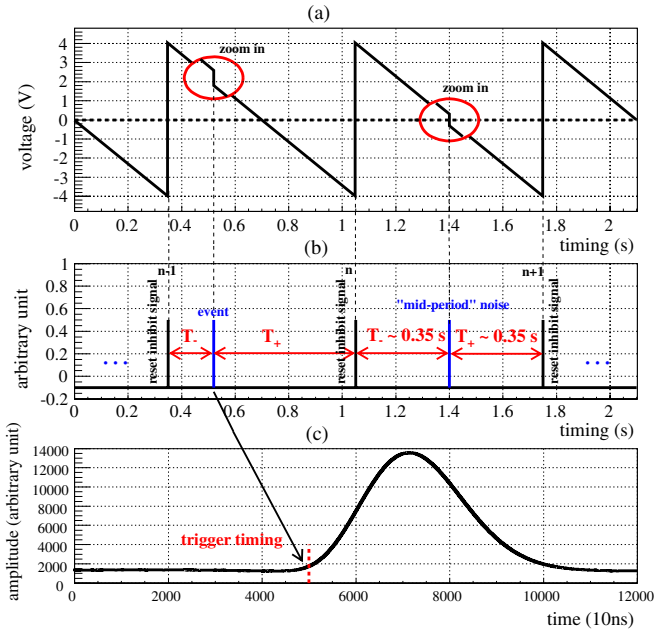

FIG. 1 (color online). Output of the PPCGe detector showing the relative timing: (a) raw signals from reset preamplifier; (b) timing of reset-inhibit and typical physics and "mid-period" noise events; (c) amplifier output with 12 μs shaping time.

A first run of 18.1 days was taken, and the DAQ dead time was 0.5% as measured by the random trigger events. We focus in this paper on the analysis of this data set. Signals coming from S_{p12} were chosen as the energy measurement. We defined the pulse area of one event as its energy. The random trigger events were used for defining the zero in energy calibration. Rectangular pulser signals with various amplitudes were injected into the test input of the preamplifier of the PPCGe detector for trigger efficiency measurement.

We used two kinds of methods to do the data selection and analysis. The first method is related to the timing information of one event. The second one is related to the characteristics of the pulse shape of one event.

In our experiment, noise events mostly occur in the middle range of the reset period while the physics events and the random trigger events are uniformly distributed. This kind of "mid-period" noise was due to the interference of the output of the preamplifier and the zero level when they are close to each other. As illustrated in Figs. 2(a) and 2(b), we denote T_- as the time interval between the event and its nearest prior-inhibit signal, and T_+ as the time interval between this event and its nearest post-inhibit signal. Figure 2(a) shows the relationship of T_- and T_+ for both random trigger events and background events. These can therefore be rejected by the "TT cut" which leads to a live time penalty. The background spectra before and after the TT cut, as well the random trigger spectra, have been shown in Figs. 2(b) and 2(c).

The pulse shape discrimination is based on two methods. The first method uses the "pedestals of $S_{p6,12}$ and T_p"

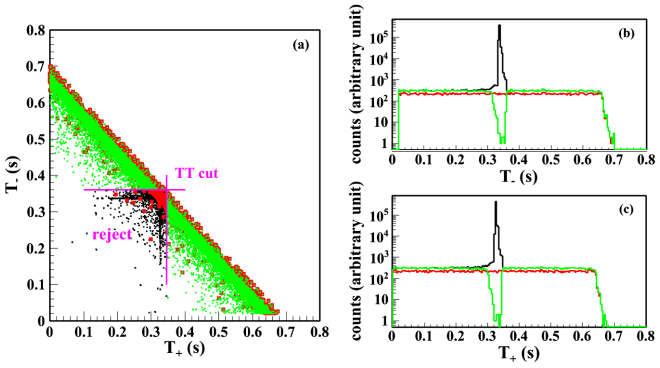

FIG. 2 (color online). The scatter plots of T_+ and T_- for random trigger events (red color) and background events before and after the TT cut (black and green color) are shown in Fig. 2(a). The TT cut has also been overlaid on the scatter plot. The spectra before and after the TT cut are given in Figs. 2(b) and 2(c); at the same time, the T_+ and T_- spectra for a random trigger have also been shown in these figures.

(Ped) cuts, which are applied to discriminate those events whose pedestals exhibit anomalous behavior. The criteria are derived from the random trigger events whose pedestal distributions are considered consistent with the physical events. The signal efficiencies for the TT and Ped cuts, which are independent of the pulse amplitude, were accurately measured with random trigger events, and are 92.5% and 96.2%, respectively. A data set of 16.0 kg-day has been obtained after the TT and Ped cuts.

The second method uses the pulse shape discrimination (PSD) cuts, which are effective approaches to reject remaining noise events, including one cut based on the correlation between the integration area and its maximum amplitude of S_{p12}, and another cut based on the correlation between signals from the p^+ electrode and n^+ electrode for one event. The efficiencies of the PSD cuts were measured by an ^{241}Am source sample and a ^{137}Cs source sample (ε_{PSD}). The spectra of the ^{241}Am source along the analysis chain are given in Fig. 3(a). The efficiencies derived

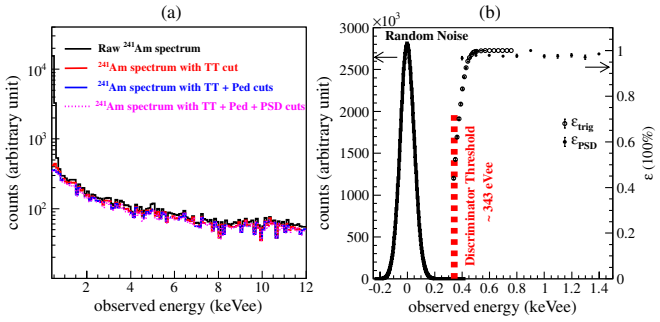

FIG. 3 (color online). The ^{241}Am spectra along the analysis chain are shown in Fig. 3(a). The distribution of the random noise fluctuation and the discriminator threshold of our hardware are given in Fig. 3(b). The trigger efficiency ε_{trig} and PSD cut efficiency ε_{PSD} have also been shown in the same plot.

from ^{241}Am and ^{137}Cs spectra agree very well, and the bin-by-bin combined ε_{PSD} are shown in Fig. 3(b). The source spectra provide measurements of the TT and Ped cut efficiencies consistent with those derived from random trigger events.

The distribution of the random noise is given in Fig. 3(b). The energy resolution at this zero energy point is 51 eVee ("ee" represents electron equivalent energy). The hardware discrimination threshold, defined at 50% trigger efficiency, is calculated to be about 343 eVee and much higher than $5 \cdot \sigma$ (255 eVee). In addition, the trigger efficiency is nearly equal to 100% above 500 eVee.

Considering both the trigger and signal selection efficiencies, the 400 eVee energy threshold is selected as our energy threshold for physical analysis. Fig. 4(a) shows the low-energy background spectrum detected by the PPCGe detector with corrections for the ε_{trig} and cuts efficiencies, fiducial mass and the dead time. Both statistic and systematic errors are considered with standard error propagation. Several characteristic x-ray peaks can be seen. They are due to the cosmogenic radioactive isotopes which are mainly generated within the germanium crystal before

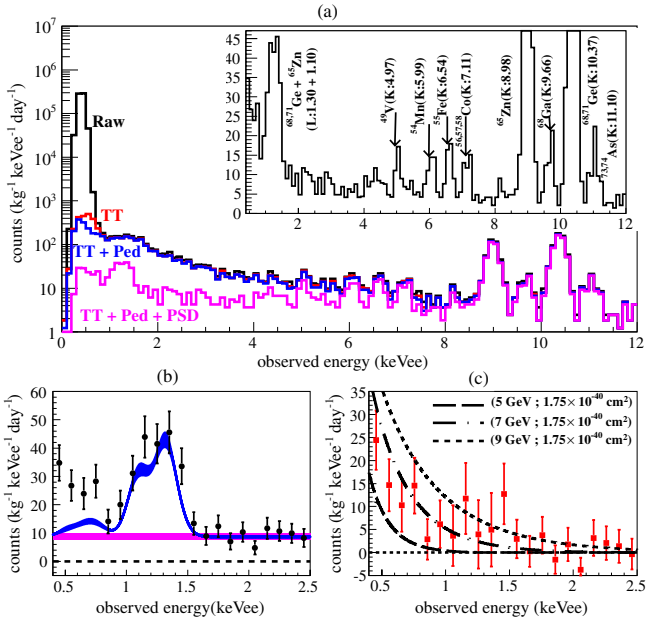

FIG. 4 (color online). The observed energy spectra showing raw data and data after the TT cut, TT + Ped cuts, and TT + Ped + PSD cuts are given in Fig. 4(a). The inset plot in Fig. 4(a) shows the background spectrum after the TT + Ped + PSD cuts with the ε_{trig}, cuts efficiencies, fiducial mass, and the dead time correction. Eight K-shell peaks for L-shell peaks predictions are identified. The low-energy spectrum in the range of 0.4–2.4 keVee is shown in Fig. 4(b), as well the calculated L-shell background contribution and the flat γ background with the expanded statistical error band. The residual spectrum is shown in Fig. 4(c), superimposed with the predicted spectra for 5, 7, and 9 GeV WIMPs with spin-independent cross section $\sigma_{\chi N} = 1.75 \times 10^{-40}$ cm^2.

installation into CJPL, and include ^{68,71}Ge, ^{68}Ga, ^{73,74}As, ^{65}Zn, and so on. Because of the 1.5 mm oxygen-free high-conductivity copper cryostat surrounding the germanium crystal, the external low-energy x-rays cannot enter into the bulk of the PPCGe detector. Energy calibration was therefore accomplished by using these internal-origin radioactive isotopes. The decays of the K-shell (10.37 keV) and L-shell (1.29 keV) peaks of ^{68,71}Ge isotopes accord well with their expected half-life [14]. As the characteristic x-rays are internal and short-ranged, the detection efficiency is almost 100%. The ratios of K-shell to L-shell x-ray events calculated based on Ref. [15] are used to predict the intensity of the L-shell in the lower energy ranges (< 2 keVee). The background spectrum in the low-energy range of 0.4–2.4 keVee and the L-shell contributions calculated from the eight clearly visible K-shell peaks is shown in Fig. 4(b).

We do not apply the surface bulk cut in this analysis. Accordingly, from simulations and previous measurements [4,6,9], there should be a flat γ spectrum contributed by the bulk γ events which is mainly located at the internal volume of a PPCGe detector and a monotonously decreasing background spectrum from anomalous surface events due to incomplete charge collection. so that the expected background should be monotonously decreasing. In addition to the L-shell x-ray contributions, a conservative flat background level was subtracted at an energy range beyond the tails of the χ-N nuclear recoil spectrum which, for $m_\chi < 12$ GeV, corresponds to 1.7–2.4 keVee. The final residual spectrum in the region of 0.4–2.4 keVee is shown in Fig. 4(c), from which the constraints on WIMPs are derived.

The thickness of the outer n^+ layer of a p-type germanium detector can be measured by a multi γ-ray isotope, such as ^{133}Ba [16]. Due to the close match in total mass and the structure between the CDEX-1 and TEXONO [9] detectors, we chose the same depth of the dead layer at 1.16 mm with an uncertainty of 10% for easy comparison. This gives rise to a fiducial mass of 905 g with an uncertainty of less than 1%, corresponding to a data size of 14.6 kg-day.

The quenching factor of the recoiled germanium nucleus is given by the TRIM program [17]. The parameters chosen for the WIMP in thermal equilibrium include Maxwellian velocity distribution with $\nu_0 = 220$ km $\cdot$ s^{-1}, the escape velocity $\nu_{\rm esc} = 544$ km $\cdot$ s^{-1}, and the local density (ρ_χ) of 0.3 GeV $\cdot$ cm^{-3}. The energy resolution of the PPCGe was derived from the calibration data and then extrapolated to the region less than 1 keVee.

The predicted spectrum of WIMP-nucleon spin-independent interaction can be evaluated. Using the standard WIMP halo assumption [18], the light-WIMP spectra corresponding to 5, 7 and 9 GeV WIMPs with spin-independent cross section $\sigma_{\chi N} = 1.75 \times 10^{-40}$ cm^2 are also put on the spectrum in Fig. 4(c).

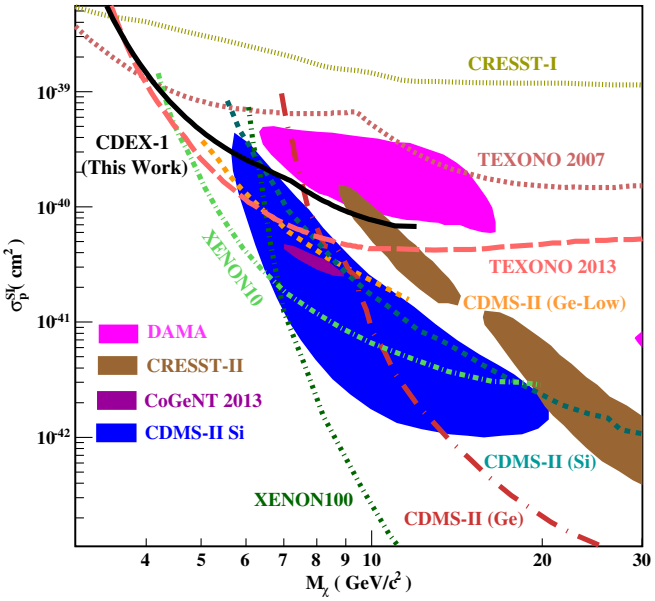

FIG. 5 (color online). Exclusion plot of spin-independent coupling, superimposed with the results from other benchmark experiments. The results are also shown in this figure including the 90% confidence regions favored by CoGeNT [4], DAMA/LIBRA [5], and CRESST-II [20], as well the exclusion limits from CDMS-II (Si) [6], XENON100, and the low-threshold analysis of XENON10 [8], TEXONO [9], and CRESST-1 [21].

Assuming all of the events from our final residual spectrum are induced by incident WIMPs, we can derive upper limits on the WIMP-nucleon spin-independent cross section at different WIMP masses. A binned Poisson method [19] is utilized, and the exclusion curve with 90% C.L. is displayed in Fig. 5, along with the results from other experiments [4–8,20]. Although we did not apply the bulk surface cut and the anti-Compton suppression, the results are close to the latest sensitivities of the TEXONO experiment [9]. The bulk surface cut could reduce the background level by a factor of 2–3 [4,9], and we expect that our new result with the bulk surface cut can be used to check these results. Also, the residual spectrum we have achieved needs to be understood further with more data.

An anti-Compton detector will be added to test its performance and background level in the regime of low cosmic ray flux. It will need to be evaluated whether the suppression power of this anti-Compton detector in CJPL can balance its additional contribution to the PPCGe's background due to its own radioactivities in detail. This will aid in the understanding of the cosmic-ray-induced background when compared with the results from Ref. [9], and it will be very helpful for the evaluation of the sensitivity of the possible future ton-scale germanium experiment in the dark matter search by the CDEX Collaboration.

This paper represents the first scientific results obtained at the new underground facilities at CJPL. The authors

would like to thank all those who contributed to its efficient construction and commissioning. We are grateful to X. Q. Li and Y. F. Zhou for useful comments. This work was supported by the National Natural Science Foundation of China (Contracts No. 10935005, No. 10945002, No. 11275107, and No. 11175099) and the National Basic Research program of China (973 Program) (Contract No. 2010CB833006).

[1] J. Beringer *et al.*, Phys. Rev. D **86**, 010001 (2012), and references therein; P. A. R. Ade *et al.*, arXiv:1303.5076v1.
[2] C. Kelso, D. Hooper, and M. R. Buckley, Phys. Rev. D **85**, 043515 (2012), and references therein.
[3] J. D. Lewin and P. F. Smith, Astropart. Phys. **6**, 87 (1996).
[4] C. E. Aalseth *et al.*, Phys. Rev. Lett. **101**, 251301 (2008); **106**, 131301 (2011); **107**, 141301 (2011); Phys. Rev. D **88**, 012002 (2013).
[5] P. Belli, R. Bernabei, A. Bottino, F. Cappella, R. Cerulli, N. Fornengo, and S. Scopel, Phys. Rev. D **84**, 055014 (2011); R. Bernabei *et al.*, Eur. Phys. J. C **67**, 39 (2010).
[6] Z. Ahmed, Science **327**, 1619 (2010); Phys. Rev. Lett. **106**, 131302 (2011); arXiv:1203.1309; R. Agnese *et al.*, arXiv:1304.3706v2; arXiv:1304.4279v2.
[7] G. Angloher *et al.*, Eur. Phys. J. C **72**, 1971 (2012).
[8] E. Aprile *et al.*, Phys. Rev. Lett. **107**, 131302 (2011); J. Angle *et al.*, Phys. Rev. Lett. **107**, 051301 (2011); E. Aprile *et al.*, Astropart. Phys. **35**, 573 (2012); Phys. Rev. Lett. **109**, 181301 (2012).
[9] S. T. Lin *et al.*, Phys. Rev. D **79**, 061101 (2009); H. B. Li *et al.*, Phys. Rev. Lett. **110**, 261301 (2013).
[10] P. N. Luke, F. S. Goulding, N. W. Madden, and R. H. Pehl, IEEE Trans. Nucl. Sci. **36**, 926 (1989).
[11] Q. Yue *et al.*, High Energy Phys. Nucl. Phys. **28**, 877 (2004); D. He *et al.*, High Energy Phys. Nucl. Phys. **30**, 548 (2006); X. Li *et al.*, High Energy Phys. Nucl. Phys. **31**, 564 (2007).
[12] K. J. Kang, J. P. Cheng, Y. H. Chen, Y. J. Li, M. B. Shen, S. Y. Wu, and Q. Yue, J. Phys. Conf. Ser. **203**, 012028 (2010); Q. Yue and H. T. Wong, J. Phys. Conf. Ser. **375**, 042061 (2012); K. J. Kang *et al.*, Front. Phys. **8**, 412 (2013).
[13] Y. C. Wu *et al.*, Chinese Phys. C **37**, 086001 (2013).
[14] K. J. Kang *et al.*, arXiv:1305.0401.
[15] J. N. Bahcall, Phys. Rev. **132**, 362 (1963).
[16] E. Aguayo *et al.*, Nucl. Instrum. Methods Phys. Res., Sect. A **701**, 176 (2013).
[17] J. F. Ziegler, Nucl. Instrum. Methods Phys. Res., Sect. B **219–220**, 1027 (2004); S. T. Lin *et al.*, Phys. Rev. D **79**, 061101 (2009).
[18] F. Donato, N. Fornengo, and S. Scopel, Astropart. Phys. **9**, 247 (1998).
[19] C. Savage, G. Gelmini, P. Gondolo, and K. Freese, J. Cosmol. Astropart. Phys. 04 (2009) 010.
[20] M. Felizardo *et al.*, Phys. Rev. Lett. **108**, 201302 (2012); S. Archambault *et al.*, Phys. Lett. B **711**, 153 (2012).
[21] G. Angloher *et al.*, Astropart. Phys. **18**, 43 (2002).